The 8th European Congress on Computational Methods in Applied Sciences and Engineering
ECCOMAS Congress 2022
5-–9 June 2022, Oslo, Norway

UNSTEADY AERODYNAMIC SENSITIVITY ANALYSIS WITH FENICS

Carlos J. Ruiz[1,*], A. Martínez-Cava Aguilar[1,2], M. Chávez-Modena[1,3] and E. Valero[1,3]

[1] Universidad Politécnica de Madrid, Plaza Cardenal Cisneros 3, E-28040 Madrid, Spain

[2] Instituto Universitario "Ignacio Da Riva" (IDR/UPM), Universidad Politécnica de Madrid, Plaza Cardenal Cisneros, 3, E-28040, Madrid, Spain

[3] CCS-UPM - Centre for Computational Simulation, Universidad Politécnica de Madrid, Boadilla del Monte, E-28660, Madrid, Spain

Key words: Unsteady flow, Sensitivity analysis, Adjoint methods, Finite Elements, FEniCS

Abstract. Sensitivity analysis is considered a fundamental tool in aerospace engineering, allowing to evaluate the impact of parameters variations, and optimize the aerodynamic and structural design. There has been much effort in the development of both theoretical and numerical frameworks for sensitivity calculations through adjoint solutions. Regarding the implementation of these analyses into agile and versatile numerical tools, the use of scalable and transferable libraries has become of particular importance.

In this work, FEniCS is used to calculate the sensitivity of aerodynamic observables in different flow condition. A comparison with different theoretical and benchmark cases is used to validate the methodology before applying it to further and more complex configurations, expanding the scope of the analyses to unsteady flows.

1 Introduction

Flow control and optimization are one of the main fields in aerospace design. The use of the adjoint method for optimization theory has a long history[1]. The first time in history that adjoint equations were used for design was in 1970 by Pironneaupironneau1974optimum, but it was not until 1988, with the help of Jameson[2, 3], that the first applications were made in the field of computational fluid dynamics, CFD. From this point on, CFD codes for optimization began to be developed, such as Huffman [4], Elliot[5].For where an exhaustive review of these early algorithms is made, see Newman[6], , and for a first look to this field, see Giles[7].

There are many geometry optimisation methods for different parameters. On the one hand, some of them are based on the discrete adjoint, i.e. first discretize and then compute the adjoint problem, see Nielsen [8] or Chen[9], but most of them on the discrete method, This way, it is much easier to formulate, but it is necessary to differentiate matrices, which implies modifying the geometry a priori, as well as losing importance on the physics of the problem. These methods are very used in the stationary case, but with great limitations in non-stationary fluids as you need to compute the derivative and for that you need to modify the mesh at each step.

In this work, we seek to obtain a formula of drag sensitivity by change on geometry, based on the continuous adjoint method, that gives us an expression from which we can extract physical information as a function of the adjoint and original variables for both stationary and non-stationary flows from the original mesh (see Section sec:TheoreticalFrame.

Once this formula has been found, the implications for both steady state and non-steady state have been studied in Section sec:Methodology. In the latter case, the effects of a deformation obtained by the mean of the sensitivity and of a deformation in each time step have been studied as a first approximation to discover the power of this expression (see Section sec:Sensitivity.

2 Theoretical Framework

To approach optimisation we have two types of problems, unconstrained and constrained. On the one hand, the goal of an unconstrained optimization problem is to find the state of the system, $\mathbf{q}$, that minimizes or maximizes a scalar of the system, the cost function , $\mathcal{J}$. We assume that $\mathcal{J}$ belongs C_∞ class, with a particular value of $\mathbf{q}$ that cancels the gradient, $\mathrm{d}\mathcal{J}/\mathrm{d}\mathbf{q}$. In most cases, this cancelation is impossible, and we can only act on a set of control parameters, $\mathbf{g}$. On the other hand, the goal of constrained optimization is to minimize or maximize the cost function, $\mathcal{J}$, by acting on $\mathbf{g}$, where $\mathbf{q}$ and $\mathbf{g}$ are subjected to $\mathbf{F}(\mathbf{q},\mathbf{g}) = 0$.

Many of the cost functionals encountered in the literature do not depend on the control variables [10]; this can lead to unbounded controls parameters. There are two different ways to compute this:

1. Constrain the size of the admissible controls,

$$||\mathbf{g}|| \leq \kappa, \tag{1}$$

   where κ is a physical parameter.

2. Penalize the objective functional: the goal is to minimize, for some defined norm and constants,

$$\mathcal{J}(\mathbf{q},\mathbf{g}) = \mathcal{E}(\mathbf{q}) + \alpha||\mathbf{g}||^\beta, \tag{2}$$

   where $\mathcal{E}(\mathbf{q})$ is a given functional.

In addition, we have to make a distinction between stationary and non-stationary problems, since the parameter to optimize do not have to depend on time, we have to integrate with respect to it and add another constraint that imposes the initial conditions.

2.1 Steady case

To calculate the sensitivity (the gradient) of the cost function, we introduce the Lagrangian functional as:

$$\mathcal{L}(\mathbf{q},\mathbf{g},\lambda) = \mathcal{J} - \lambda \cdot \mathbf{F}(\mathbf{q},\mathbf{g}), \tag{3}$$

where λ is the adjoint variable. A variation of the Lagrangian follows the expression:

$$\delta\mathcal{L} = \frac{\partial\mathcal{L}}{\partial\mathbf{q}}\delta\mathbf{q} + \frac{\partial\mathcal{L}}{\partial\mathbf{g}}\delta\mathbf{g} + \frac{\partial\mathcal{L}}{\partial\lambda}\delta\lambda \tag{4}$$

The extreme condition are enforced on, since the Langrangian reaches an extremum if $\delta\mathcal{L} = 0$ for all variations, therefore the following conditions on the derivatives are imposed:

$$\begin{aligned} \frac{\partial \mathcal{L}}{\partial \mathbf{q}} &= \mathbf{0}, \\ \frac{\partial \mathcal{L}}{\partial \mathbf{g}} &= \mathbf{0}, \\ \frac{\partial \mathcal{L}}{\partial \lambda} &= \mathbf{0}. \end{aligned} \tag{5}$$

Developing these derivatives from Equation (3), we obtain the following expressions:

$$\nabla_{\mathbf{q}}\mathcal{L} := \frac{\partial \mathcal{L}}{\partial \mathbf{q}} = \frac{\partial \mathbf{F}}{\partial \mathbf{q}}^T \lambda - \frac{\partial \mathcal{J}}{\partial \mathbf{q}} = \mathbf{0}, \tag{6}$$

$$\nabla_{\mathbf{g}}\mathcal{L} := \frac{\partial \mathcal{L}}{\partial \mathbf{g}} = \frac{\partial \mathbf{F}}{\partial \mathbf{g}}\lambda - \frac{\partial \mathcal{J}}{\partial \mathbf{g}} = \mathbf{0}, \tag{7}$$

$$\nabla_{\lambda}\mathcal{L} := \frac{\partial \mathcal{L}}{\partial \lambda} = -\mathbf{F} = \mathbf{0}. \tag{8}$$

The equation (6) is the adjoint equation, the equation (7) the optimization equation over g and the equation (8) is the state equation.

2.2 Unsteady case

Unlike the steady case, in the unsteady case the state equation depends on time,

$$\mathbf{F}(\mathbf{q}(t), \mathbf{g}, t) = \frac{\mathrm{d}\mathbf{q}}{\mathrm{d}t} - \mathbf{N}(\mathbf{q}, \mathbf{g}, t) = \mathbf{0} \tag{9}$$

with a initial condition $\mathbf{F_0}(\mathbf{q}, \mathbf{g}, t_0) = \mathbf{q}(0) - \mathbf{q}_0 = \mathbf{0}$.

The Lagrangian can be defined as

$$\mathcal{L} = \mathcal{J} - \int_{t_0}^{T} (\lambda \cdot \mathbf{F}) dt - \mu \cdot \mathbf{F}_0. \tag{10}$$

The optimization system is derived by setting to zero the variation of the Lagrangian with respect to all variables, like the steady case, recovering the optimization system.

3 Description of the problem

To validate the methodology, we consider a two-dimensional circular cylinder immersed in an incompressible laminar flow. The physical domain is $\Omega\{(x, y)|\ x \in [-40D, 50D],\ y \in [-40D, 40D]\}/\Gamma$ where D is the diameter of the cylinder set to one and Γ denotes the surface of the cylinder defined by the following expression $\Gamma = \{(x, y)|x^2 + y^2 < D^2\}$. The fluid density, ρ, and the kinematic viscosity, ν, are assumed constant; therefore, the non-dimensional parameter for this problem is the Reynolds number, $\mathrm{Re} = \frac{u_\infty D}{\nu}$, where u_∞ is the free-stream velocity. The evolution of the fluid is ensured by the steady Navier-Stokes equations,

$$\frac{\partial \mathbf{u}}{\partial t} + \mathbf{u} \cdot \nabla \mathbf{u} - \nabla \cdot \sigma(p, \mathbf{u}) = \mathbf{f},\ \nabla \cdot \mathbf{u} = \mathbf{0},\ \text{ in } \Omega, \tag{11}$$

with boundary conditions $\mathbf{u} = \mathbf{g}$ on Γ, $\mathbf{u} = (1, 0)$ at the inflow and walls , $p\mathbf{n} - \frac{1}{\mathrm{Re}}\nabla\mathbf{u} = \mathbf{0}$, at the outflow , where $\mathbf{n}$ the normal vector on the surface, and σ is the stress tensor, defined as

$$\sigma(p, \mathbf{u}) = -pId + \frac{1}{\mathrm{Re}}(\nabla\mathbf{u} + \nabla^T\mathbf{u}). \tag{12}$$

Combining the Equation (10) and Equation (11), we obtain the Lagrangian of our problem to calculate the drag sensitivity is defined as

$$\mathcal{L} = \overline{D} - \frac{1}{T}\int_0^T \int_\Omega \mathbf{u}^\dagger \cdot (\frac{\partial \mathbf{u}}{\partial t} + \mathbf{u}\cdot\nabla\mathbf{u} - \nabla\cdot\sigma(p, \mathbf{u}) - \mathbf{f})\mathrm{d}\Omega\mathrm{d}t - \frac{1}{T}\int_0^T \int_\Omega p^\dagger \nabla\cdot\mathbf{u}\mathrm{d}\Omega\mathrm{d}t \tag{13}$$

where $\overline{D} = \frac{2}{T}\int_0^T \int_\Gamma \sigma(\mathbf{u}, p)n \cdot \mathbf{e}_x \mathrm{d}\Gamma\mathrm{d}t$ is the mean drag force.

3.1 Mesh validation

The mesh composed of triangular elements is generated using FEniCS with two refinements, first over $\{(x, y)|\ x \in [-9D, 24D],\ y \in [-9D, 9D]\}$ and the second over $\{(x, y)|\ x \in [-3D, 12D],\ y \in [-3D, 3D]\}$.

The first step is to ensure the independence of the solution from the mesh. For this purpose, different fundamental quantities of two-dimensional flow over a circular cylinder have been compared with reference data for steady [11, 12] and unsteady [13] flow.

First, for steady flow at Re = 40, the computed quantities are the drag coefficient and the bubble separation point measured on the cylinder surface. The comparison of the variation of the drag with the number of elements we and for separation angle of the bubble, see

ΩΩimmediateñe:db@cref

ΩΩimmediateñe:db@cref

	Drag coefficient	Bubble separation ($^{\mathrm{o}}$)
Reference	1.5187	53.50
Present	1.516	53.52

Table 1: Comparation of drag coefficient and bubble separation point at Re = 40.

On the other hand, in the non-stationary regime, Re = 100 we have calculated both the Strouhal number and the mean drag. For the Strouhal number, $\mathrm{St} = \frac{fD}{U_\infty}$, a point of the wake has been selected, in particular the point $(x, y) = (6, 0)$ of the mesh, and the variation of the vertical velocity has been studied. For the mean drag when we obtain the St. The results are shown in Table 2.

	Strouhal number	Mean drag coefficient
Reference [13]	0.166	1.336
Present	0.1636	1.334

Table 2: Comparison of the Strouhal number and mean drag at Re = 100

l_x	l_y	n_Γ	n
$[-40, 50]$	$[-40, 40]$	1280	11700

Table 3: Details of the computational mesh in the analysis

3.2 Validation of calculation of sensitivitiesin several cases

Now, we validate the implementation on FEniCS in two cases, in both steady and non-steady state regimes.

3.2.1 Drag sensitivity by a external force in Steady case

We know $\nabla_f D = \mathbf{u}^\dagger$, see Wang et al.[14], with its respective equation for $\mathbf{u}^\dagger$. For this validation, we impose the next conditions: We set Re $= 20$, the external force $\mathbf{f} = \mathbf{0}$ and the boundary condition around the cylinder $\mathbf{g} = \mathbf{0}$. In Figure 1, we can see the comparison of the gradient of the drag obtained by Wang et al.[14] with present work. The magnitude of the field tells us which zones are most efficient at modifying the drag.

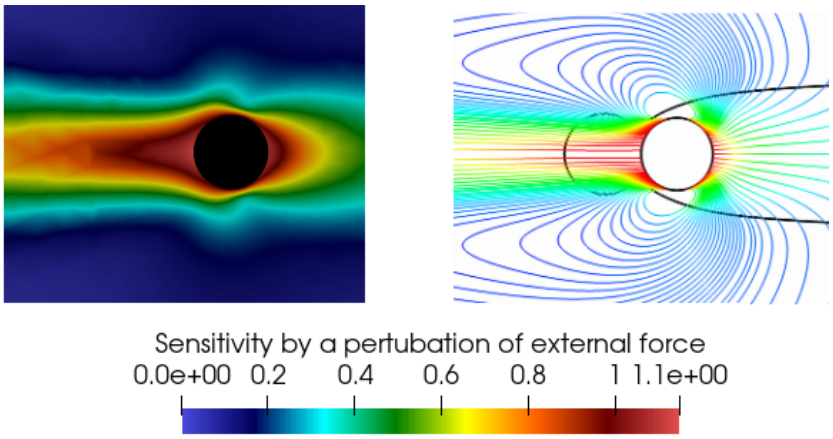

Figure 1: Comparison of the sensitivity to perturbations in the external force. Same scale has been used in both images.

3.3 Unsteady flow

For the unsteady analysis, we need to store each time step of the unsteady flow solution to solve the adjoint equations backward in time. We impose a Reynolds number of Re $= 100$. This flow regime, the wake presents a Von-Kármán vortex shedding, and solve the Navier-Stokes equations for $(\mathbf{u}, p)$, storing the solution for every steps. In these simulations, we used a time step of $\Delta t = 0.016s$ to solve Navier-Stokes equations, we use the Chorin's method[15]. Once all the solutions of the temporary window have been stored, 145 seconds, solving the adjoint equations with the same time step backward in time.

We have analyzed the physics of the problem starting from having a developed wake and after reaching periodical convergence conditions, when we have a dominant frequency in the wake.

In the following sections, we have calculated the sensitivity of drag in different situations and compared with the literature to validate our methodology.

3.3.1 Drag sensitivity by a perturbation on the boundary condition around the cylinder

In this section, we have calculated the sensitivity by a perturbation on the boundary condition and compared the results with Meliga et al.[13]. We look for the gradient of

$$\overline{D} = \frac{2}{T}\int_0^T \int_\Gamma \{\sigma(p,\mathbf{u})n \cdot \mathbf{e}_x\} \mathrm{d}\Gamma \mathrm{d}t. \tag{14}$$

For this problem, we set the external force $\mathbf{f} = \mathbf{0}$ and the boundary condition around the cylinder $\mathbf{g} = \mathbf{0}$. Applying these conditions, we get a expression to the sensitivity of the drag force to a perturbation of the boundary condition around the cylinder [13],

$$\nabla_{\mathbf{g}} \overline{D} = \sigma(-p^\dagger, \mathbf{u}^\dagger)\mathbf{n}. \tag{15}$$

In **??** and Figure 2, we observe the evolution of the sensitivity around a period of the vortex. The first snapshot describes a suction distribution over the upper half of the cylinder surface, together with a blowing of lesser magnitude over the lower half. The third snapshot unveils the same pattern of substantial suction and lesser blowing, only both halves of the cylinder surface exchange roles because the phase is shifted by half a shedding period. The transition from one pattern to the other is accompanied by a distortion of the blowing velocity at the rear surface, found to be stronger on the half of the cylinder at which suction is applied, and by an almost constant blowing on the front surface.

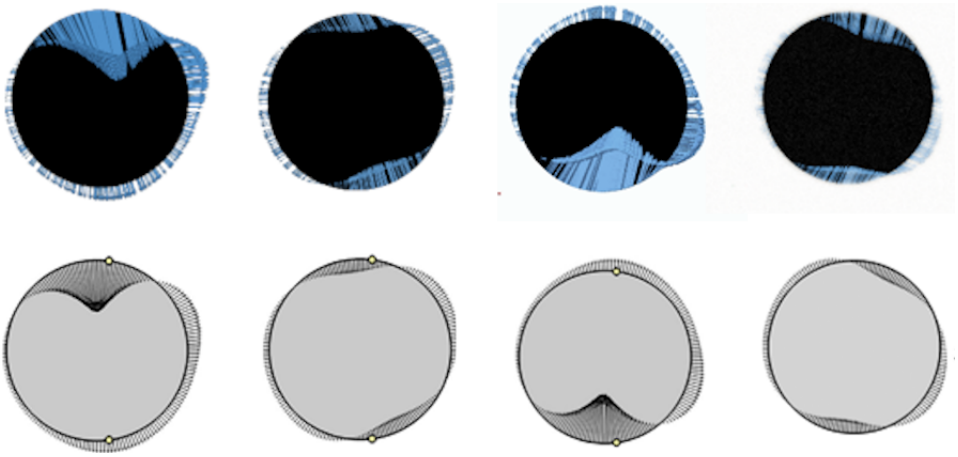

Figure 2: Temporal evolution of a period sensitivity at Re = 100. Results of [13]

3.3.2 Drag sensitivity by a external force

In this case, we have calculated sensitivity by a external force and compared the results obtained with Wang et al.[14]. For the sensitivity by a external force, we use the equation

$$\nabla_{\mathbf{f}} \overline{D} = \mathbf{u}^{\dagger} \tag{16}$$

set the external force $\mathbf{f} = \mathbf{0}$ and the boundary condition around the cylinder $\mathbf{g} = \mathbf{0}$. Figure 3 illustrates the evolution of the adjoint field, colored by the magnitude of the adjoint velocity. We show three time snapshots covering about half of a period and the comparison with Wang et al. Observe how the sensitivity is changing from the upper to the lower of the cylinder every half period of the vortex, in addition to a second zone that is generated approximately one diameter away from the cylinder and that is approaching it.

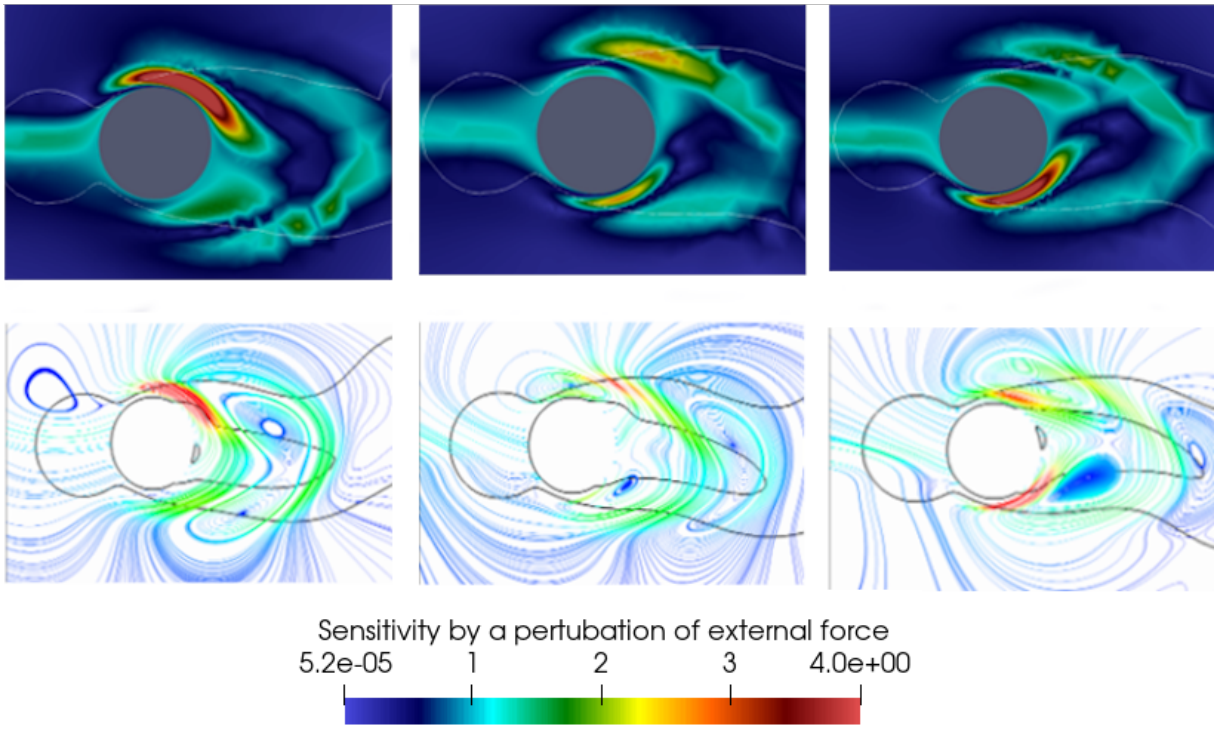

Figure 3: Comparison of the sensitivity to perturbations in the external force at Re = 100.

4 Sensitivity of frag force by shape change

The objective is to obtain an analytical formula that gives us the sensitivity to changes in geometry from which we can obtain an interpretation of the physics of the problem.

Once we have managed to calculate the sensitivity to changes in the boundary condition, we can use it to calculate the sensitivity to changes in geometry, need the following theorem, See Gunzburger[10] or Sokolowski[16]:
Let Γ_0 the initial boundary, $(\mathbf{u}, p)$ the solution of Navier-Stokes equations, and Γ' a perturbation

on the boundary. The perturbation flow, $(\mathbf{u}', p')$ induced by the variation of the boundary satisfies the linearized Navier- Stokes's equations with the following boundary condition on the cylinder:

$$\mathbf{u}' = -\frac{\partial \mathbf{u}}{\partial \mathbf{n}}(\mathbf{v} \cdot \mathbf{n}) \tag{17}$$

where $\mathbf{v}$ is defined by $\Gamma_0 - \Gamma'$. That is, at first order, we have an identification of a perturbation in the geometry with one in the initial conditions.

If we apply this result to the sensitivity to boundary conditions, we can obtain the following expression for sensitivity to changes in geometry,

$$\nabla_\Gamma D = \langle \sigma(-p^\dagger, \mathbf{u}^\dagger)\mathbf{n}, -\frac{\partial \mathbf{u}}{\partial \mathbf{n}} \rangle \mathbf{n} \tag{18}$$

This equation is derived assuming that the boundary condition is now $\mathbf{g} = 0$, since we focus only on changes to the geometry of the immersed body.

Looking at the above equation, we see that the sensitivity to changes in geometry is nothing more than the projection of the sensitivity to perturbation at the boundary condition on the cylinder onto the normal derivative of the velocity on the surface $\nabla_\Gamma D = \langle \nabla_{\mathbf{g}} D, -\frac{\partial \mathbf{u}}{\partial \mathbf{n}} \rangle \mathbf{n}$.

4.1 Steady flow

In this flow regime,we set the Reynolds number to 40, the external force $\mathbf{f} = \mathbf{0}$ and the boundary condition around the cylinder $\mathbf{g} = \mathbf{0}$. In Figure 4 we have a representation of the drag sensitivity around the cylinder. How the sensitivity gives us information on where and in which direction the deformations affect drag the most. If we induce a variation where we move each point in the direction of the sensitivity at that point, we obtain a new shape, see Figure 5.

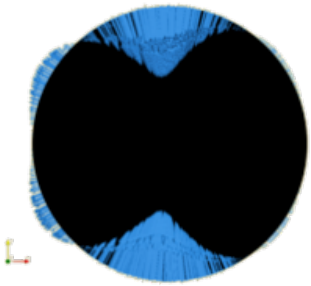

Figure 4: Steady Sensitivity by geometry changes

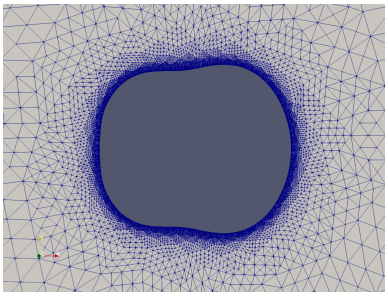

Figure 5: Mesh deformed by 5% of the magnitude of sensitivity

Table 5 shows data on various deformations and respective drag reductions.

Figure 6 shows the flow using both the original and deformed geometries. In addition, we observe a small decrease in the size of the recirculation bubble.

4.2 Unsteady flow

This section includes the non-stationary case at Re = 100 with $\mathbf{f} = \mathbf{0}$, and $\mathbf{g} = \mathbf{0}$. Two different simulation are done with different deformation obtained through Equation (18). First,

Deformation(%)	Drag reduction (%)
1	2.3
2	3.6
5	7.2

Table 4: Drag reduction as a function of the percentage of the magnitude of the sensitivity.

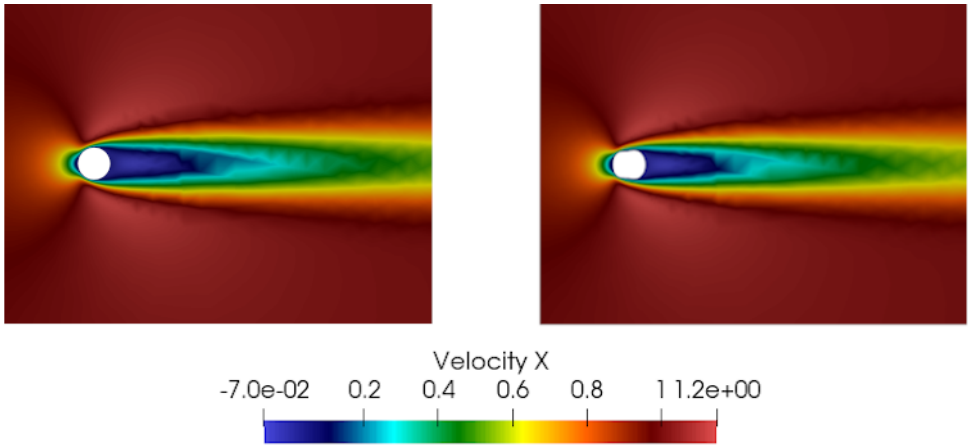

Figure 6: Horizontal velocity in the original geometry and in the deformed geometry (5%).

by taking the time average of all the deformations, $\frac{1}{T}\int_0^T \nabla_{\mathbf{g}} D \mathrm{d}t$, and second by deforming at each time step according to the equation and study the effect of each of them on the drag behaviour.

4.2.1 Mean deformation

First we will focus on studying the physics of flow using the mean deformation, as depicted in Figure 7, for 0.5, 1 and $2\%\nabla_\Gamma D$.. The function that governs the deformation is the time average of the sensitivity. In addition to a reduction of the mean drag, but also, as we increase the deformation, we obtain a reduction of the oscillation amplitude of the drag. Table 5 shows how the mean drag decreases as a function of the deformation. Figure 8 we can see the behaviour of the drag for different deformations, depending on the percentage that we impose

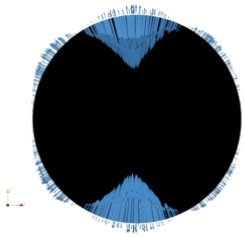

Figure 7: Mean deformation function

on the sensitivity.

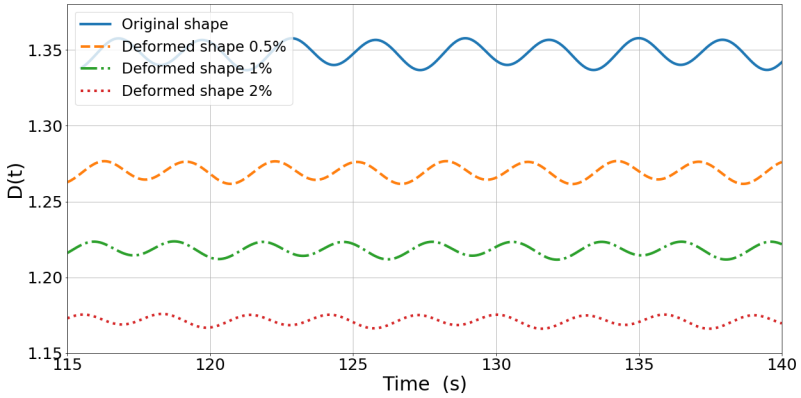

Figure 8: Evolution of drag by several mean deformations

Deformation(%)	Drag reduction (%)
0.5	7,2
1	9.5
2	14

Table 5: Mean drag reduction as a function of the percentage of the magnitude of the mean sensitivity

4.2.2 Instantaneous deformation

For this analysis, we deform the mesh at each time step by obeying the time-dependent sensitivity. We can see the behaviour of the function in Figure 9. The images correspond to 4 equispaced snapshots of the period of the function where the magnitude indicates how efficient it is to deform in that direction.

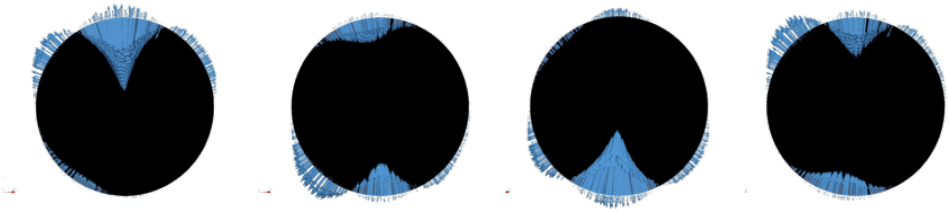

Figure 9: Results:Temporal evolution of a period sensitivity.

Using an instantaneous deformation, Figure 10 shows that for a deformation of 0.2% both

the drag and the oscillation amplitude decrease very little, but when we increase the percentage more, although the drag decreases, the oscillation amplitude increases.

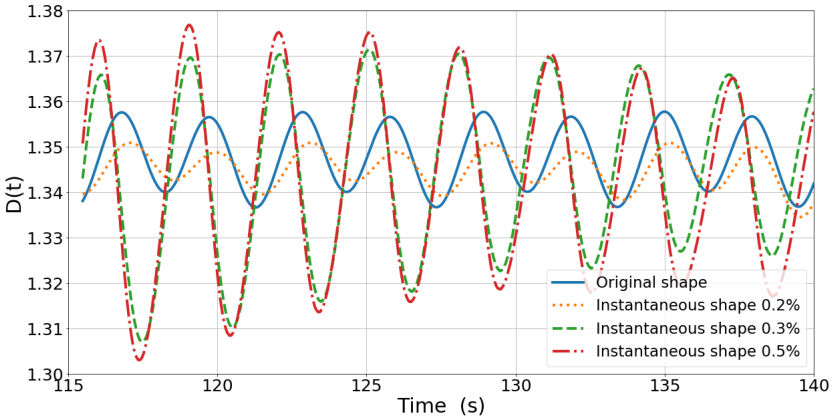

Figure 10: Evolution of drag by several instantaneous deformations

5 Conclusions

Thanks to the bijection between a perturbation in the shape and in the boundary condition on the cylinder, we have found a physical expression of the sensitivity to changes in the geometry and its relation to the sensitivity to a perturbation in the boundary condition. In the stationary case, we can see that with small deformations we have obtained a substantial reduction of the drag coefficient, as well as a reduction of the size of the recirculation bubble.

Within the analysis of the non-stationary fluid, we have observed that the application of the mean deformation is more efficient than applying a specific deformation at each time step.

Our next objectives are focused on improving the results obtained using instantaneous deformation with different approaches to pursue industrial applications such as morphing wings.

REFERENCES

[1] D. Edmunds, Optimal control of systems governed by partial differential equations (1972).

[2] A. Jameson, Aerodynamic design via control theory, Journal of scientific computing 3 (3) (1988) 233–260.

[3] A. Jameson, Optimum aerodynamic design using cfd and control theory, in: 12th computational fluid dynamics conference, 1995, p. 1729.

[4] W. Huffman, R. Melvin, D. Young, F. Johnson, J. Bussoletti, M. Bieterman, C. Hilmes, Practical design and optimization in computational fluid dynamics, in: 23rd Fluid Dynamics, Plasmadynamics, and Lasers Conference, 1993, p. 3111.

[5] J. Elliott, J. Peraire, Practical three-dimensional aerodynamic design and optimization using unstructured meshes, AIAA journal 35 (9) (1997) 1479–1485.

[6] J. C. Newman III, A. C. Taylor III, R. W. Barnwell, P. A. Newman, G. J.-W. Hou, Overview of sensitivity analysis and shape optimization for complex aerodynamic configurations, Journal of Aircraft 36 (1) (1999) 87–96.

[7] M. B. Giles, N. A. Pierce, An introduction to the adjoint approach to design, Flow, turbulence and combustion 65 (3) (2000) 393–415.

[8] E. J. Nielsen, B. Diskin, Discrete adjoint-based design for unsteady turbulent flows on dynamic overset unstructured grids, AIAA journal 51 (6) (2013) 1355–1373.

[9] W. Chen, C. Gao, Y. Gong, W. Zhang, Shape optimization to improve the transonic fluid-structure interaction stability by an aerodynamic unsteady adjoint method, Aerospace Science and Technology 103 (2020) 105871.

[10] M. D. Gunzburger, Perspectives in flow control and optimization, SIAM, 2002.

[11] O. Posdziech, R. Grundmann, A systematic approach to the numerical calculation of fundamental quantities of the two-dimensional flow over a circular cylinder, Journal of fluids and structures 23 (3) (2007) 479–499.

[12] S. Sen, S. Mittal, G. Biswas, Numerical simulation of steady flow past a circular cylinder, in: Proceedings of the 37th National & 4th International Conference on Fluid Mechanics and Fluid Power December, Vol. 16, 2010.

[13] P. Meliga, E. Boujo, M. Meldi, F. Gallaire, Revisiting the drag reduction problem using adjoint-based distributed forcing of laminar and turbulent flows over a circular cylinder, European Journal of Mechanics-B/Fluids 72 (2018) 123–134.

[14] Q. Wang, J.-H. Gao, The drag-adjoint field of a circular cylinder wake at reynolds numbers 20, 100 and 500, Journal of Fluid Mechanics 730 (2013) 145–161.

[15] A. J. Chorin, A numerical method for solving incompressible viscous flow problems, Journal of computational physics 135 (2) (1997) 118–125.

[16] J. Sokolowski, J.-P. Zolésio, Introduction to shape optimization, in: Introduction to shape optimization, Springer, 1992, pp. 5–12.